



## Development of a numerical 2-dimensional beach evolution model

**Baykal, Cüneyt**

*Published in:*  
Turkish Journal of Earth Sciences

*Link to article, DOI:*  
[10.3906/yer-1302-1](https://doi.org/10.3906/yer-1302-1)

*Publication date:*  
2014

*Document Version*  
Publisher's PDF, also known as Version of record

[Link back to DTU Orbit](#)

*Citation (APA):*  
Baykal, C. (2014). Development of a numerical 2-dimensional beach evolution model. *Turkish Journal of Earth Sciences*, 23(2), 215-231. <https://doi.org/10.3906/yer-1302-1>

---

### General rights

Copyright and moral rights for the publications made accessible in the public portal are retained by the authors and/or other copyright owners and it is a condition of accessing publications that users recognise and abide by the legal requirements associated with these rights.

- Users may download and print one copy of any publication from the public portal for the purpose of private study or research.
- You may not further distribute the material or use it for any profit-making activity or commercial gain
- You may freely distribute the URL identifying the publication in the public portal

If you believe that this document breaches copyright please contact us providing details, and we will remove access to the work immediately and investigate your claim.

## Development of a numerical 2-dimensional beach evolution model\*

Cüneyt BAYKAL\*\*\*

Section of Fluid Mechanics, Coastal and Maritime Engineering, Department of Mechanical Engineering,  
Technical University of Denmark, Kongens Lyngby, Denmark

Received: 03.02.2013

Accepted: 07.11.2013

Published Online: 18.01.2014

Printed: 17.02.2014

**Abstract:** This paper presents the description of a 2-dimensional numerical model constructed for the simulation of beach evolution under the action of wind waves only over the arbitrary land and sea topographies around existing coastal structures and formations. The developed beach evolution numerical model is composed of 4 submodels: a nearshore spectral wave transformation model based on an energy balance equation including random wave breaking and diffraction terms to compute the nearshore wave characteristics, a nearshore wave-induced circulation model based on the nonlinear shallow water equations to compute the nearshore depth-averaged wave-induced current velocities and mean water level changes, a sediment transport model to compute the local total sediment transport rates occurring under the action of wind waves, and a bottom evolution model to compute the bed level changes in time based on the gradients of sediment transport rates in cross-shore and longshore directions. The developed models are applied successfully to the SANDYDUCK field experiments and to some conceptual benchmark cases including simulation of rip currents around beach cusps, beach evolution around a single shore perpendicular groin, and a series of offshore breakwaters. The numerical model gave results in agreement with the measurements both qualitatively and quantitatively and reflected the physical concepts well for the selected conceptual cases.

**Key words:** Spectral waves, nearshore circulation, sediment transport, beach evolution

### 1. Introduction

The continuous geomorphological evolution of coastal areas is the result of a dynamic and highly complex balance between the anthropogenic activities at coastal areas and various physical processes occurring due to the interactions between the 3 masses of earth: land, water, and atmosphere. Among these processes, the sediment transport due to wind wave action plays an important role in this evolution. The prediction of this evolution for various temporal and spatial scales and for various types of problems such as erosion/accretion around coastal structures, navigation channels, river mouths, or tidal inlets has been of great concern for scientists and engineers for decades. Starting from the 1950s until the present, numerous researchers have attempted to model nature both physically and numerically to understand and predict temporal and spatial morphological changes at coastal areas. Numerical modeling of beach evolution was first studied by Pelnard-Considere (1956), who introduced the one-line theory for the prediction of shoreline changes next to a groin. This study was later followed by many others to develop 1-dimensional shoreline change models

with extended capabilities (Hanson and Kraus, 1989; Dabees and Kamphuis, 1998; Danish Hydraulic Institute, 2001). Over the years, advances in computer technology and numerical modeling techniques encouraged the development of more sophisticated 2-dimensional (2D) and 3-dimensional (3D) tools for the investigation of morphological changes in further detail compared to 1-dimensional models.

Basically, 2D or 3D models are composed of several separate models for the computation of wave transformation, nearshore current, sediment transport, and bottom evolution. Quasi-3D (Q3D) models or fully 3D models are more preferable for short-term events (less than 1 year) where the vertical distribution of current velocities and concentrations become important for accurate modeling. A Q3D model is simply a 2D horizontal (2DH) model with an additional 1-dimensional vertical profile model (1DV) to include the effects of return flows (undertow) in cross-shore dynamics (Briand and Kamphuis, 1993). A fully 3D model solves the governing hydrodynamic equations in 3 dimensions (Warner et al., 2008). The 2DH or 2D vertical (2DV) models require less

\* Correspondence: cbaykal@gmail.com

\*\* On leave from Department of Civil Engineering, Middle East Technical University, Ankara, Turkey

computational load compared to 3D models and provide the simulation of longer-term events (Shimizu et al., 1996). Some of the recent studies on 2DH modeling of beach evolution are those of Militello et al. (2004), Buttolph et al. (2006), Kuroiwa et al. (2006), Bruneau et al. (2007), Roelvink et al. (2009), and Nam et al. (2009, 2010).

Militello et al. (2004) and later Buttolph et al. (2006) developed the M2D model (later called CMS-M2D) for simulating the nearshore hydro- and morphodynamics such as currents due to waves, tides, wind, and rivers; sediment transport; and morphology changes. The model is a 2D depth-averaged (2DH) model solving nonlinear shallow water equations (NSWEs) for nearshore currents and including sediment transport, hard-bottom, and avalanching modules. The model is coupled with STWAVE or WABED for the wave forcings. Kuroiwa et al. (2006) proposed a hybrid predictive model of 3D beach evolution with shoreline changes, based on depth-averaged current (2DH) and Q3D current models. They used Mase's (2001) spectral wave model with the formulation of Takayama et al. (1991) for the energy dissipation term. The current model utilizes the mixing terms related to Dally et al.'s (1984) energy dissipation rate. The authors applied their model to some theoretical cases, field observations on bar movements, and a medium-term beach evolution problem due to a fishing port. Bruneau et al. (2007) constructed a 2DH nearshore morphology model coupling the spectral wave model SWAN with a NSWE model MARS (Perenne, 2005) and a sediment transport module based on MORPHODYN (Saint-Cast, 2002). The authors applied their model only to some theoretical cases with complex bathymetrical features. Roelvink et al. (2009) developed a 2DH numerical nearshore model, called XBeach, to simulate hydrodynamics and morphological changes in the surf and swash zones during storms and hurricanes, including dune erosion, overwash, and breaching. XBeach consists of a wave transformation model based on action balance equation, a flow model based on NSWEs, a sediment transport model solving the advection-diffusion equation for the depth-averaged concentrations, bottom evolution, and avalanching modules to predict the morphological changes during storm events. The model has been validated through several analytical, laboratory, and field case studies (Roelvink et al., 2009). Recently, Nam et al. (2009, 2010) developed a 2DH nearshore morphology model for simulating nearshore waves, currents, sediment transport, and bottom changes. The authors used Mase's (2001) spectral wave model with Dally et al.'s (1985) energy dissipation term, a surface roller (Dally and Brown, 1995; Larson and Kraus, 2002), and a nearshore current model (Militello et al., 2004).

## 2. Beach evolution model

### 2.1. Model structure

The main objective of this study is to construct a 2D beach evolution numerical model based on the available methodologies in the literature that is computationally less demanding and mainly applicable to medium- to long-term (days, years) and meso- to macroscale (hundreds of meters to kilometers) morphological changes at coastal areas, i.e. beach evolution problems around coastal defense structures.

The 2DH BeaCh EvOlution Numerical MoDel (COD) constructed in this study is mainly composed of 4 submodels: the Nearshore Spectral Wave Model (NSW), NearShore Circulation Model (NSC), SEDiment Transport Model (SED), and Bottom EVolution Model (EVO). The numerical model is developed in MATLAB utilizing finite difference schemes to the numerical solutions of the governing equations of the above submodels. The main inputs of the COD are the offshore or nearshore wave conditions (wave height, period, approach angle, and directional spreading of the waves), the initial nearshore sea bottom and land topographies (including coastal structures), and the controlling model parameters based on case specific conditions such as breaker index, median grain size diameter, diffraction intensity parameter, and turbulent eddy viscosity. The model structure is given in Figure 1.

As shown in Figure 1, in the numerical modeling of beach evolution, the first step is to set the case-specific controlling parameters, initial bathymetry, offshore wave conditions, and grid and time spacing. The second step is to compute nearshore wave heights, mean wave directions, maximum orbital velocities at the bottom, and radiation stress terms for the given wave condition around existing coastal defense structures over the initial irregular bathymetry. The computed wave-related parameters are assumed to be constant during the given wave condition. The third step is to compute the growth and decay of kinetic energies of surface rollers (vortices occurring in front of breaking waves), the friction and radiation terms obtained from the outputs of the wave, and surface roller models. Using these terms, the time- and depth-averaged local nearshore wave-induced current velocities and mean water level changes for the given wave condition over the initial bathymetry are computed in this step. In the fourth step, the computed nearshore current velocities and wave-related parameters are used in the computation of depth-averaged total sediment transport rates both in cross-shore and longshore directions. Finally, the computed sediment transport rates are used in the continuity equation to update the bathymetry, and new bathymetry is used for the succeeding wave conditions.

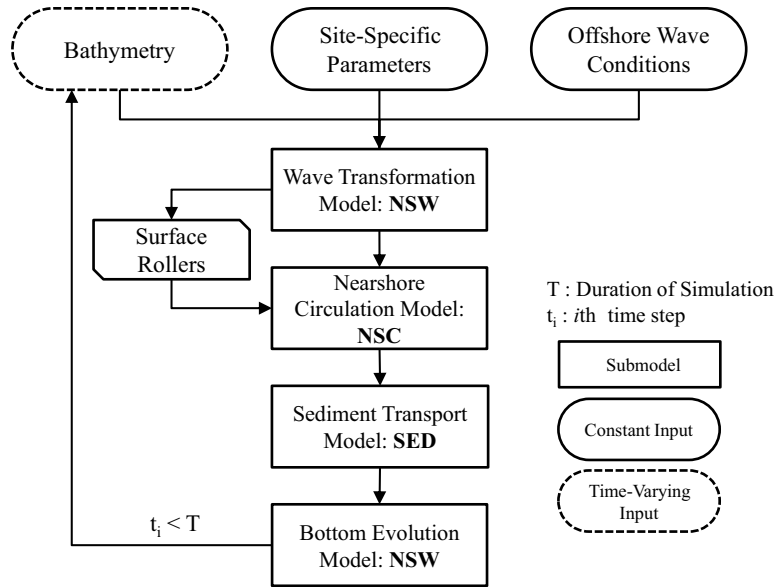


Figure 1. Beach evolution numerical model (COD) structure.

## 2.2. Nearshore Spectral Wave Model: NSW

The nearshore wave model is a phase-averaged spectral wave model, i.e. the variation of wave parameters within a wave period or during the time series of irregular wave trains is disregarded. NSW solves the energy balance equation over an arbitrary bathymetry and in the angular domain only. Nearshore wave parameters are assumed to be constant during the duration of the wave condition, which might be selected as 1 h, or the duration of a single storm or the occurrence in hours in a year from a particular direction. To reduce the computational demand in the numerical modeling of wave transformation, the energy distribution over the frequency domain is disregarded, and the directional random waves are represented with the peak wave period only. The directional spreading of the waves is defined from  $-\pi/2$  to  $+\pi/2$  with a cosine power '2s' distribution given by Mitsuyasu et al. (1975). Wave transformation over the arbitrary bathymetry and around structures considers linear wave shoaling and refraction, depth-induced random wave breaking, and irregular wave diffraction processes only. The random waves in the surf zone are assumed to possess a full Rayleigh distribution where the wave classes in the distribution greater than a maximum depth limited wave height are assumed to be broken (Baldock et al., 1998; Janssen and Battjes, 2007). Wave-current and wave-wave interactions are not considered in the computations. Wave reflection from shore due to bottom gradients or from coastal structures, dissipation due to bottom friction, white-capping (i.e. steepness controlled dissipation in deep water) and bottom vegetation, transfer of wind energy, and Coriolis effects are

not included, yet are considered as future updates to the model.

Mase (2001) gives the energy balance equation with the additional terms for breaking and diffraction as:

$$\frac{\partial(v_x S)}{\partial x} + \frac{\partial(v_y S)}{\partial y} + \frac{\partial(v_\theta S)}{\partial \theta} = D_b - D_d \quad (1)$$

where  $S$  is the directional wave spectral density (in  $m^2/\text{rad}$ ) that varies in  $x$  and  $y$  horizontal coordinates (cross-shore and longshore directions, respectively; Figure 2) and with respect to  $\theta$ , the angle measured counterclockwise from the  $x$ -axis.  $D_b$  is the dissipation rate due to random wave breaking and  $D_d$  is the diffraction term introduced by Mase (2001). The propagation velocities ( $v_x$ ,  $v_y$ ,  $v_\theta$ ) are given as:

$$(v_x, v_y) = (C_g \cos \theta, C_g \sin \theta) \quad (2)$$

$$v_\theta = \frac{C_g}{C} \left( \sin \theta \frac{\partial C}{\partial x} - \cos \theta \frac{\partial C}{\partial y} \right) \quad (3)$$

where  $C_g$  is the group velocity and  $C$  is the wave celerity (both in m/s), both of which are computed using linear wave theory in the numerical model. Mase (2001) introduced the wave diffraction term,  $D_d$ , to include the wave diffraction process in action/energy balance models as:

$$D_d = \frac{\kappa}{2\omega} \left( (CC_g \cos^2 \theta \cdot S_y)_y - \frac{1}{2} CC_g \cos^2 \theta \cdot S_{yy} \right) \quad (4)$$

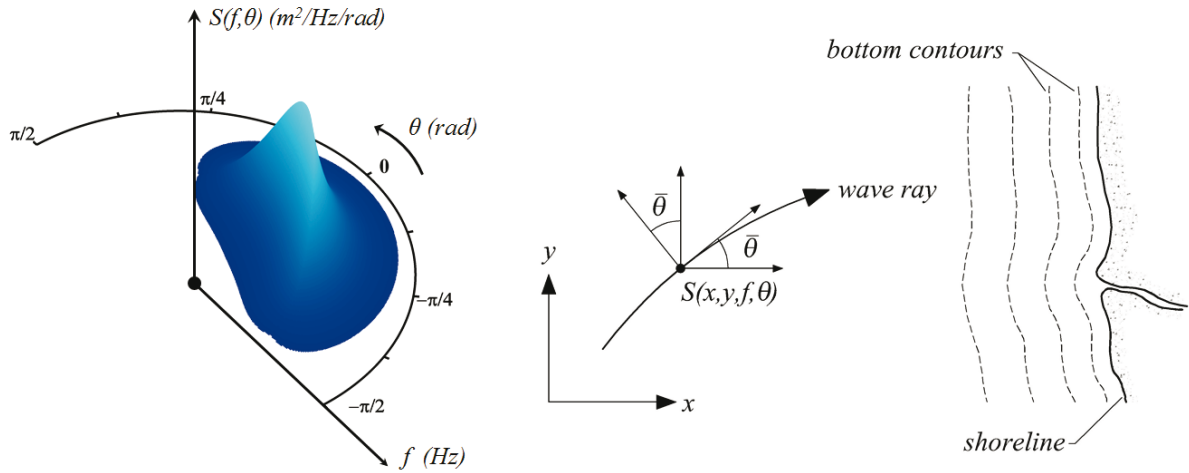


**Figure 2.** Coordinate system used in the numerical model (after Mase, 2001).

where  $\kappa$  ( $\geq 0$ ) is the diffraction intensity parameter, stated to be equal to 2.5 by Mase (2001) in the absence of field or laboratory data, and  $\omega$  is the angular wave frequency.

Dissipation of wave energy flux due to random wave breaking in the numerical model is described with the methodology given by Janssen and Battjes (2007), which is based on the method proposed by Baldock et al. (1998). In this method, the distribution of random waves in the surf zone is assumed to be a full Rayleigh distribution with a weighting function that assumes that the waves greater than a maximum depth limited wave height are broken. The given method satisfies the condition that the fraction of broken waves cannot exceed unity at the shoreline even for steep beaches, where there is not enough time for all of the incident wave energy to be dissipated and an unsaturated breaking condition exists. The dissipation rate of wave energy flux ( $D_b$ ) due to random wave breaking is given as follows:

$$D_b = B \frac{3\sqrt{\pi}}{16} f \frac{H_{rms}^3}{h} \left\{ 1 + \frac{4}{3\sqrt{\pi}} \left[ \left( \frac{H_b}{H_{rms}} \right)^3 + \frac{3}{2} \left( \frac{H_b}{H_{rms}} \right) \right] \cdot \exp \left[ - \left( \frac{H_b}{H_{rms}} \right)^2 \right] - \operatorname{erf} \left( \frac{H_b}{H_{rms}} \right) \right\} \quad (5)$$

where  $B$  is a tunable parameter to control the intensity of the dissipation (taken as unity),  $H_{rms}$  is the root mean square (rms) wave height at water depth  $h$ ,  $\operatorname{erf}$  is the error function, and  $H_b$  is the maximum depth-limited wave height ( $H_b = \gamma_b \times h$ ), where  $\gamma_b$  is the breaker index. The  $f$  in the above given equation is defined as the representative

wave frequency by Janssen and Battjes (2007) and it is assumed to be equal to the peak frequency  $f_p$  in this study.

The arbitrary bathymetry is discretized using a Cartesian coordinate system, where  $x$  is the cross-shore direction and  $y$  is the longshore direction. Similarly, the angular domain of the spectral density is discretized into finite angular grids. In the numerical solution of Eq. (1), a first-order backwards scheme in the  $x$ -direction, first-order centered scheme in the  $y$ -direction, and angular domain are utilized, yielding an explicit up-winding scheme in the cross-shore direction and an implicit scheme for the unknown density components in longshore direction and angular domain. Three types of boundary conditions are used in the solution: offshore, open sea, and dissipative beach boundary conditions. The offshore boundary condition is of the Dirichlet type, where the offshore wave conditions are defined. The open sea boundary condition is of the Neumann type, where the water depth is greater than a minimum water depth ( $h_{min}$ ). The dissipative beach boundary condition (dry points: land, islands, and structures) is applied at the grid cells where the water depth is less than  $h_{min}$  at any location of the computational area. The spectral densities at these boundaries are assumed to be equal to zero. No specific boundary condition is applied at reflective boundaries such as coastal structures or steep beaches as the wave reflection from coastal structures or steep beaches is neglected.

### 2.3. Nearshore Circulation Model: NSC

Nearshore local current velocities and mean water level changes are computed solving the 2D depth-averaged NSWE, of which the main assumption is that the water depth ( $h$ ) is small compared to the wavelength ( $L$ ;  $L/h > 20$ ), in addition to the inviscid and incompressible fluid

assumptions. This means that the vertical accelerations of the fluid particles are negligible and the pressure distribution is hydrostatic over the flow depth. This assumption is often violated for short waves in shallow water depths. The vertical structure of the cross-shore current velocities is disregarded. Thus, undertow in the surf zone, which significantly affects the bar formation, is not taken into consideration. This assumption limits the model applicability where the cross-shore movement of sediments governs the morphological changes such as short-term events. In the surf zone, part of the dissipated wave energy due to wave breaking is assumed to be used in the growth and decay of kinetic energies of surface rollers. Effects of surface rollers both in cross-shore and longshore directions are included in the nearshore circulation computations. Effects of tidal, wind, and Coriolis terms are disregarded as the effects of such mechanisms are often negligible compared to wave forcing over small- to medium-scale areas, respectively (up to tens of kilometers). In the numerical model, NSWs are solved until reaching a steady state solution for a given wave condition, during which the nearshore wave conditions over the computational domain are assumed to be constant.

Near shore wave-induced current velocities and changes in mean sea level are computed by solving NSWs, which are basically conservation mass and momentum in  $x$ - and  $y$ -directions. NSWs are given as:

$$\frac{\partial \eta}{\partial t} + \frac{\partial}{\partial x} [u(h+\eta)] + \frac{\partial}{\partial y} [v(h+\eta)] = 0 \quad (6)$$

$$\frac{\partial u}{\partial t} + u \frac{\partial u}{\partial x} + v \frac{\partial u}{\partial y} + g \frac{\partial \eta}{\partial x} + \frac{1}{\rho(h+\eta)} [\tau_{bx} + F_x] - A_x = 0 \quad (7)$$

$$\frac{\partial v}{\partial t} + u \frac{\partial v}{\partial x} + v \frac{\partial v}{\partial y} + g \frac{\partial \eta}{\partial y} + \frac{1}{\rho(h+\eta)} [\tau_{by} + F_y] - A_y = 0 \quad (8)$$

where  $t$  is time (in seconds);  $u$  and  $v$  are the depth-averaged current velocities in the  $x$  (cross-shore) and  $y$  (longshore) directions, respectively;  $\eta$  is the change in mean sea level;  $h$  is the water depth from still water level;  $\rho$  is the density of water (typically taken as  $\rho = 1025 \text{ kg/m}^3$  for salt water and  $\rho = 1000 \text{ kg/m}^3$  for fresh water);  $g$  is the gravitational acceleration ( $g = 9.81 \text{ m/s}^2$ );  $\tau_{bx}$  and  $\tau_{by}$  are the bottom shear stresses;  $F_x$  and  $F_y$  are the sum of radiation stresses and stresses acting on the water body due to surface rollers; and  $A_x$  and  $A_y$  are the lateral mixing stresses. The  $F_x$  and  $F_y$  terms are the governing stress terms in this set of equations. Goda (2010) gives the wave-induced stress terms,  $F_x$  and  $F_y$ , as:

$$F_x = \left[ \left( \frac{\partial S_{xx}}{\partial x} + \frac{\partial S_{xy}}{\partial y} \right) + \frac{\partial}{\partial x} (2E_{sr} \cos^2 \bar{\theta}) + \frac{\partial}{\partial y} (E_{sr} \sin 2\bar{\theta}) \right] \quad (9)$$

$$F_y = \left[ \left( \frac{\partial S_{yx}}{\partial x} + \frac{\partial S_{yy}}{\partial y} \right) + \frac{\partial}{\partial x} (E_{sr} \sin 2\bar{\theta}) + \frac{\partial}{\partial y} (2E_{sr} \sin^2 \bar{\theta}) \right] \quad (10)$$

where  $S_{xx}$ ,  $S_{xy}$ ,  $S_{yx}$ , and  $S_{yy}$  are the radiation stress terms;  $E_{sr}$  is the kinetic energy of the surface roller; and  $\bar{\theta}$  is the mean approach angle with respect to the  $x$  axis, positive in a counter-clockwise direction. Tajima and Madsen (2003) give the kinetic energy of the surface rollers ( $E_{sr}$ ) with the following equation:

$$E_{sr} = \frac{\rho A_{sr} C}{2T} \quad (11)$$

where  $A_{sr}$  is the surface roller area,  $C$  is the wave celerity, and  $T$  is the wave period, which is taken as the peak wave period ( $T_p$ ) in the numerical model. The evolution of the kinetic energy of surface roller over an arbitrary bathymetry is given as

$$\alpha \rho g \left[ \frac{\partial}{\partial x} (m_0 C_g \cos \bar{\theta}) + \frac{\partial}{\partial y} (m_0 C_g \sin \bar{\theta}) \right] + \left[ \frac{\partial}{\partial x} (E_{sr} C \cos \bar{\theta}) + \frac{\partial}{\partial y} (E_{sr} C \sin \bar{\theta}) \right] = - \frac{K_{sr} E_{sr} C}{h} \quad (12)$$

where  $\alpha$  is the energy transfer coefficient (varies between 0 and 1) controlling the transferred energy to the surface roller,  $m_0$  is the total wave energy density, and  $K_{sr}$  is the energy dissipation rate of the surface roller. Tajima and Madsen (2003) relate  $K_{sr}$  to the bottom slope ( $m$ ) as follows:

$$K_{sr} = \frac{3}{8} (0.3 + 2.5m) \quad (13)$$

In the numerical model, the bottom shear stress terms,  $\tau_{bx}$  and  $\tau_{by}$ , are computed with the following equations given by Longuet-Higgins (1970) due to their simplicity in use compared to many other expressions.

$$\tau_{bx} = \frac{4}{\pi} \cdot \rho \cdot c_f \cdot u \cdot u_0 \quad (14)$$

$$\tau_{by} = \frac{2}{\pi} \cdot \rho \cdot c_f \cdot v \cdot u_0 \quad (15)$$

In the above equations,  $c_f$  is the friction coefficient varying between 0.005 and 0.010,  $u$  and  $v$  are the depth-averaged wave-induced current velocities, and  $u_o$  is the maximum horizontal orbital velocity at the sea bottom. The lateral mixing terms,  $A_x$  and  $A_y$ , in the  $x$ - and  $y$ -directions, respectively, are given with the following equations:

$$A_x = \frac{\partial}{\partial x} \left[ \mu \frac{\partial u}{\partial x} \right] + \frac{\partial}{\partial y} \left[ \mu \frac{\partial u}{\partial y} \right] \quad (16)$$

$$A_y = \frac{\partial}{\partial x} \left[ \mu \frac{\partial v}{\partial x} \right] + \frac{\partial}{\partial y} \left[ \mu \frac{\partial v}{\partial y} \right] \quad (17)$$

where  $\mu$  is the turbulent eddy viscosity term. Goda (2006) compared the effect of the available expressions for turbulent eddy viscosity (Longuet-Higgins, 1970; Battjes, 1975; Larson and Kraus, 1991) on the cross-shore profiles of longshore currents on planar beaches and recommended the empirical expression given by Larson and Kraus (1991) for practical applications:

$$\mu = \Lambda u_o H_{rms} \quad (18)$$

where  $\Lambda$  is an empirical constant taking values between 0.1 and 3.0 (Ding et al., 2006).

Prior to the solution of the NSW numerically, the stress terms are evaluated first. The radiation stress terms, maximum horizontal orbital velocities, total wave energy densities, mean approach angles, and significant and rms wave heights are obtained from the outputs of the wave transformation model. As the next step, the kinetic energies of surface rollers over the arbitrary bathymetry are computed solving the equation of evolution of surface roller kinetic energy. An implicit finite difference scheme is employed in the numerical solution of Eq. (12). At the offshore boundary condition,  $E_{sr}$  is assumed to be equal to zero as the random wave breaking has not started yet. At the lateral (open sea) boundaries, the rates of change of  $E_{sr}$  in the  $x$ - and  $y$ -directions are assumed to be constant. At dry points, where the water depth is less than  $h_{min}$ ,  $E_{sr}$  is assumed to be equal to zero again.

In the numerical solution of NSWs, an explicit scheme of 2 time steps of the Lax and Wendroff (1960) finite difference method on a staggered grid system is used (Burkardt, 2010). The steady state is controlled with user-defined tolerance values for each unknown parameter. To satisfy the numerical stability, the time step ( $\Delta t$ ) is defined with the following expression for 2D rectangular grids (Syme, 1991):

$$\Delta t \leq \frac{\min(\Delta x, \Delta y)}{\sqrt{2g \max(h)}} \quad (19)$$

where  $\Delta x$  and  $\Delta y$  are the grid spaces in the  $x$ - and  $y$ -directions, respectively, and  $h$  is the water depth (positive for wet points).

As for the boundary conditions, at the offshore boundary where the wave conditions are defined, the mean water level is set to zero. At the offshore and open sea boundaries, the velocity component gradients are set to zero. At the dry cells,  $u$ ,  $v$ , and  $\eta$  are assumed to be equal to zero. Moreover, at the wet cells neighboring dry cells, such as shoreline, or the wet cells around structures and the wet cells with a very steep bottom slope (e.g., bottom slopes steeper than 1:10),  $u$ ,  $v$ , and  $\eta$  are assumed to be the average of the values of the neighboring cells to overcome the instability problems close to the structures and the moving boundary condition at the shoreline.

#### 2.4. Sediment Transport Model: SED

The sediment transport model computes the local sediment transport rates under the action of wind waves over the arbitrary bathymetry to be used in the computation of bottom evolution. Sediment transport rates are computed for noncohesive sediments and are phase-averaged. Therefore, the presence of phase shift between sediment and water motions is not considered. The asymmetry in the oscillatory flow, mostly noticeable outside the surf zone under relatively calm weather conditions, is also disregarded. In this study, for the computation of sediment transport rates, the Watanabe (1992) formulation is used. The method is based on the shear stress concept (or power model concept) where the total load both in cross-shore and longshore directions ( $q_{total,x}$  and  $q_{total,y}$  in bulk volume including pores) is proportional to the residual between the mean bed shear stress under wave-current field ( $\tau_{b,cw}$ ) over a wave-cycle and the critical bed shear stress ( $\tau_{cr}$ ) that is required to mobilize the sediment grains at the sea bed

$$q_{total,x} = \frac{A \cdot [\tau_{b,cw} - \tau_{cr}] \cdot u}{\rho \cdot g} \quad (20)$$

$$q_{total,y} = \frac{A \cdot [\tau_{b,cw} - \tau_{cr}] \cdot v}{\rho \cdot g} \quad (21)$$

The empirical parameter ( $A$ ) in the above equations is given as 0.5 for monochromatic waves and 2.0 for random waves. The current velocities  $u$  and  $v$  are the depth-averaged wave-induced current velocities in cross-shore and longshore directions. The critical shear stress for incipient motion is given as:

$$\tau_{cr} = (\rho_s - \rho) \cdot g \cdot d_{50} \cdot \theta_{cr} \quad (22)$$

where  $\rho_s$  and  $\rho$  are the densities of sediment grains and water, respectively;  $g$  is the gravitational acceleration;  $d_{50}$

is the median grain diameter; and  $\theta_{cr}$  is the critical Shields parameter (see Fredsoe and Deigaard, 1994). Bijker (1971) gives the mean bed shear stress over a wave-cycle as:

$$\tau_{b,cw} = \frac{1}{T} \int_0^T \tau_{cw} \cdot dt \approx \tau_c + \frac{1}{2} \tau_{w,max} \quad (23)$$

where  $T$  is the wave period,  $\tau_c$  is the bed shear stress due to steady current  $u_c$ , and  $\tau_{w,max}$  is the maximum bed shear stress due to waves only. The bed shear stress due to depth-averaged wave-induced resultant current ( $u_c$ ) is given as:

$$\tau_c = \frac{1}{8} \rho \cdot f_c \cdot (u_c)^2 \quad (24)$$

where  $f_c$  is the current friction factor computed using the method of Van Rijn (1990). The maximum bed shear stress due to waves is given by:

$$\tau_{w,max} = \frac{1}{2} \rho \cdot f_w \cdot (u_0)^2 \quad (25)$$

where  $f_w$  is the wave friction factor computed using the method of Nielsen (1992).

## 2.5. Bottom Evolution Model: EVO

In the bottom evolution model (EVO), the gradients of the computed local total sediment transport rates both in longshore and cross-shore directions are used to compute the bed level changes in time. The depth change in time can be given with the following continuity equation:

$$\frac{\partial h}{\partial t_m} = \left( \frac{\partial q_{total,x}}{\partial x} + \frac{\partial q_{total,y}}{\partial y} \right) \quad (26)$$

where  $t_m$  is the morphological time,  $q_{total,x}$  and  $q_{total,y}$  are the phase-averaged local total sediment transport rates in terms of bulk volume transported per unit area at the cell, and  $\Delta x$  and  $\Delta y$  are the grid spacing in the  $x$ - and  $y$ -directions, respectively.

As the changes in the water depths are computed, the bottom slopes over the arbitrary bathymetry are controlled against the exceedance of a limiting slope at which the sand grains begin to roll. This critical slope is referred to as the angle of repose (or internal angle of friction). The angle of repose is given as 32–34° for dry sands and may reduce to 18° under wave action (Reeve et al., 2004; Roelvink et al., 2009).

The exceedance of the critical slope results in bottom avalanche at the sea bottom. In order to take the bottom avalanching into account in the model, an algorithm based on the work of Buttolph et al. (2006) and Roelvink et al. (2009) is followed. After every morphological time

step ( $\Delta t_m$ ), for all cells, the bottom slopes in 4 directions (in positive and negative  $x$ - and  $y$ -directions) with the neighboring cells are computed. Starting from the bottom slope in the negative  $x$ -direction in a clockwise direction, the 4 bottom slopes are checked. If 1 of the 4 bottom slopes is greater than or equal to the user-defined critical slope and the other 3 slopes, the avalanching is assumed to take place in the direction of the steepest slope and the water depths and the bottom slopes are recomputed. This control process is repeated iteratively until all the critical slopes are eliminated and the water depths at which avalanching took place are reevaluated for the respective morphological time step. In the bottom evolution computations, nonerodible bottoms are disregarded. The overall beach area, where the sediment transport rates are computed (all the wet points and the wet-dry boundary), is assumed to be eroded infinitely by the end of the simulation and there exists no hard substrate under the surface of the bathymetry. Further details about the numerical model and COD, and a detailed literature review on specific physical processes, were given by Baykal (2012).

## 3. Model validation studies

### 3.1. Field experiments: SANDYDUCK experiments (Miller, 1999)

The SANDYDUCK experiments were conducted at the US Army Engineer Waterways Experiment Station, Coastal Engineering Research Center (USACE), Field Research Facility (FRF), located in Duck, NC, USA (Miller, 1999) to investigate nearshore sediment transport processes during moderate storm conditions (individual wave heights up to 5 m and spilling breakers). The location and nearshore bathymetry of the study area was given both by Birkemeier et al. (1997) and Miller (1999). The sediment grain size distribution for the site is given as bimodal with a main component of around 0.25 mm and a secondary component near 1.0 mm. In the bar-trough region, sediment grain size distribution is given as unimodal, with a median grain size of 0.17 mm. At the seaward of the bar-trough region, the sediments are well sorted, with a median diameter of 0.12 mm (Miller, 1999). The sediment density is given as 2650 kg/m<sup>3</sup>, the sea water density is given as 1025 kg/m<sup>3</sup>, and the porosity is given as 0.4. During the experiments, the bed load and sediment load in the swash zone are not measured, but it is likely that the measured transport rates in the sampled zone include most of the transport. Bayram et al. (2001) stated that the sediment transport for all SANDYDUCK experiments is in the sheet flow regime (highly concentrated suspended sediment transport) in the surf zone, which occurs under storm conditions. The wave heights, longshore and cross-shore current velocities, and suspended sediment concentrations at various water depths along the cross-shore profile 15 m away from the pier



pilings and at water depths of up to 9 m were measured by a vertical array of instruments attached to the lower boom of a track-mounted crane. The offshore wave conditions were measured with a (directional) pressure gauge array located at a depth of 8 m (8 m array; slightly offshore and north of the FRF pier) and approximately at a cross-shore distance of 915 m with respect to the FRF coordinate system and a directional wave rider 3 km offshore at 17.4 m of water depth. The offshore wave conditions based on 8-m array measurements are given in Table 1 (Miller, 1999; Van Rijn, 2004). In the benchmark studies, both the NSW and NSC computations were carried out starting from deep water. The deep water wave conditions resulting in the offshore wave conditions are given in Table 2.

For the experiments listed in Table 1, nearshore wave heights were computed by the NSW model for the best-fitting breaker index values and the significant breaking wave heights. The fall velocity of the sand grains having a 0.17-mm median grain size diameter was computed using the method given by Ahrens (2000). The bottom friction and surface roller energy transfer coefficients and eddy viscosity constant were selected so as to give the best predictions of the longshore current velocities both qualitatively and quantitatively. Since the available data include only measured nearshore beach profiles instead of overall bathymetries at the time of experiments, the model simulations were carried out for the respective profile of each experiment. The bottom contours were assumed to be parallel to the shoreline and the existence of the pier was disregarded. The breaker index values, the controlling parameters, and the significant breaking heights and the corresponding breaker angles used in the simulations are given in Table 3.

The computed and measured nearshore significant wave heights and longshore current velocities and the

nearshore beach profiles used in the computations are given in Figures 3–11. The computed wave heights with the 2D wave transformation model are denoted by ‘NSW’ and the computed longshore current velocities with the 2D depth-averaged nearshore circulation model are denoted by ‘NSC’ in Figures 3–11.

Figures 3–11 show that the computed nearshore wave heights and the longshore current velocities are in agreement with the measured data both qualitatively and quantitatively, especially for the 19–20 October 1997 and 4 February 1998 experiments. Overall, the correlation coefficients ( $R^2$ ) between the measured and computed wave heights and longshore current velocities were found to be 0.92 and 0.50, respectively. The disparities between the measured and computed longshore velocities are mostly due to the accuracy of the computed wave height gradients and the numerical scheme used in the model. The disparities between the measured and computed wave heights might be attributed mainly to the changing offshore wave conditions during the experiments and the accuracy and the resolution of the available dataset. Moreover, the performance of the wave model and the random wave breaking method utilized depends mainly on the bottom profile and the wave steepness in the absence of significant ambient currents. As the computed longshore current velocities shows larger disparities, measured current velocities are used instead in the computation of the distributed sediment fluxes to isolate the validation of the sediment model. The A coefficient in the Watanabe (1992) formulation is taken as 2.0 for the SANDYDUCK experiments. The computed and measured local total longshore sediment fluxes are given in Figures 12–16.

Figures 12–16 show that the computed sediment flux values with the Watanabe formulation are in agreement with the measured values both qualitatively and

**Table 1.** Offshore wave conditions based on 8-m array wave measurements (Miller, 1999; Van Rijn, 2004).

Date	Mean bottom slope, 1/m	Offshore sig. wave height, $H_s$ (m)	Peak wave period, $T_p$ (s)	Offshore mean approach angle, $\bar{\theta}$ (°)
11 March 1996	1:74.8	2.8	7	10
27 March 1996	1:71.6	1.8	6.7	25
2 April 1996	1:85.3	1.6	7	26
31 March 1997*	1:69.7	1.5	7	39
1 April 1997	1:71.6	2.7	9	18
19 October 1997	1:73	3	10	20
20 October 1997*	1:76.8	2.2	11	7
4 February 1998	1:60.1	3.8	11	20
5 February 1998*	1:77.2	3.1	12	8

\*: Wave parameters for these dates are approximated from the available 8-m array and 17-m wave rider measurements.

**Table 2.** Deep water wave conditions used in the NSW model simulations.

Date	Deep water sig. wave height, $H_s$ (m)	Deep water mean approach angle, $\bar{\theta}$ (°)	Peak wave period, $T_p$ (s)	Deep water sig. wave steepness, $s_{os}$	Direc. spread. par., $s_{max}$
11 March 1996	3.02	16.0	7	0.044	3.8
27 March 1996	2.42	34.0	6.7	0.038	8.2
2 April 1996	1.82	37.0	7	0.026	24.2
31 March 1997	1.7	51.0	7	0.025	26.6
1 April 1997	3.2	29.5	9	0.028	22.0
19 October 1997	3.66	33.4	10	0.026	24.7
20 October 1997	2.16	13.4	11	0.013	57.5
4 February 1998	3.82	35.0	11	0.022	30.1
5 February 1998	3.58	17.1	12	0.018	40.1

Note: The directional spreading parameters are read from the figure given by Goda (2010) for the relationship between the deep water wave steepness and the maximum directional spreading parameter.

**Table 3.** The controlling parameters used in the NSW and NSC model simulations.

Date	Breaker index, $\gamma_{br}$ (best fit)	Breaker index, $\gamma_{br,N90}$	Bottom friction coef., $c_f$	Eddy viscosity constant, $\Lambda$	Energy transfer coef., $\alpha$	Sig. breaking wave height, $H_s$ (m)	Mean breaking approach angle, $\bar{\theta}$ (°)
11 March 1996	0.60	0.797	0.003	1.0	0.8	2.29	5.3
27 March 1996	0.60	0.764	0.005	0.5	0.3	2.12	18.2
2 April 1996	0.69	0.673	0.008	0.8	0.4	1.60	17.5
31 March 1997	0.64	0.657	0.008	0.8	0.4	1.48	31.2
1 April 1997	0.72	0.687	0.0035	0.8	0.2	2.71	12.8
19 October 1997	0.60	0.669	0.0035	1.2	0.8	3.02	15.2
20 October 1997	0.60	0.536	0.0025	1.1	0.4	2.30	5.6
4 February 1998	0.62	0.636	0.006	1.2	0.8	3.36	14.3
5 February 1998	0.45	0.589	0.003	0.5	0.5	2.54	6.8

quantitatively. Baykal et al. (2012) reported that 75% of the predicted data lie within a factor of 0.5–2.0 of the measured values with a mean absolute percent error increase of up to 65%. The correlation coefficient computed for the dataset was found to be  $R^2 = 0.54$ . The major deviations from the measured values were observed for the plunging wave cases, where the abrupt changes in wave heights were observed close to bar locations due to maximized dissipation rates of breaking waves. These disparities might be mainly attributed to the dissipation rates computed by the NSW model and the accuracy and the resolution of field measurements. It should also be noted that the results are specific to the selected controlling parameters of the model (breaker index, a parameter in the distributed load computations and directional spreading) that are not actually measured, but are selected based on engineering intuition within the given range of each parameter.

### 3.2. Conceptual benchmarks

In order to observe the behavior of the numerical beach evolution model, several simulations were performed for the conceptual cases. The first case in the conceptual benchmark studies is the modeling of rip currents around beach cusps under perpendicular wave approach. The second case is the modeling of beach evolution next to a groin perpendicular to an initially straight shoreline under oblique wave approach. The third and fourth cases are the modeling of beach evolution in the lee of a T-type groin and a series of offshore breakwaters, respectively.

#### 3.2.1. Rip currents around beach cusps (Park and Borthwick, 2001)

To study the nearshore wave-induced circulation in case of arbitrary bathymetries, a conceptual benchmark study was carried out based on Park and Borthwick's (2001) study on nearshore currents at a sinusoidal beach, which is similar

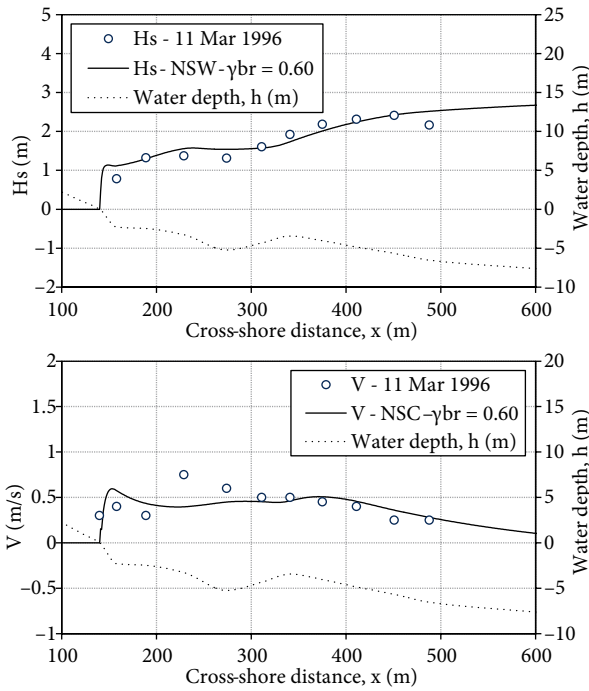


**Figure 3.** The measured and computed significant wave heights ( $H_s$ ) and longshore current velocities ( $V$ ) for the SANDYDUCK 11 March 1996 experiment.

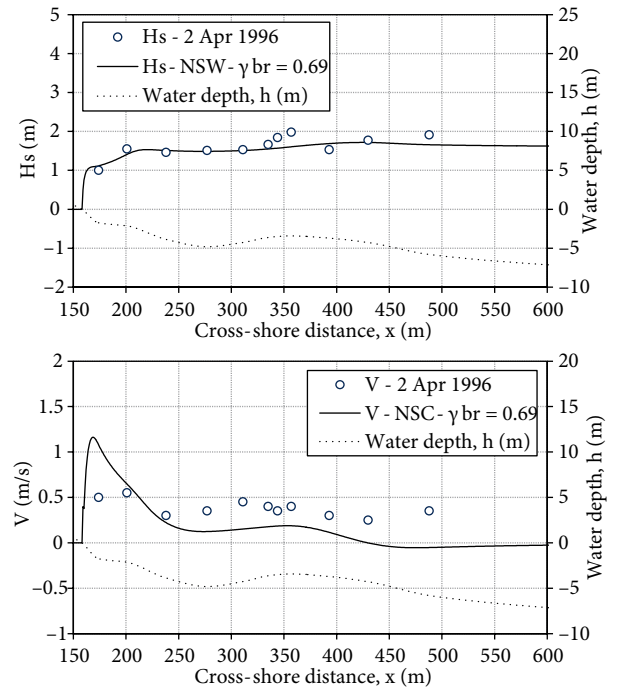


**Figure 5.** The measured and computed significant wave heights ( $H_s$ ) and longshore current velocities ( $V$ ) for the SANDYDUCK 2 April 1996 experiment.

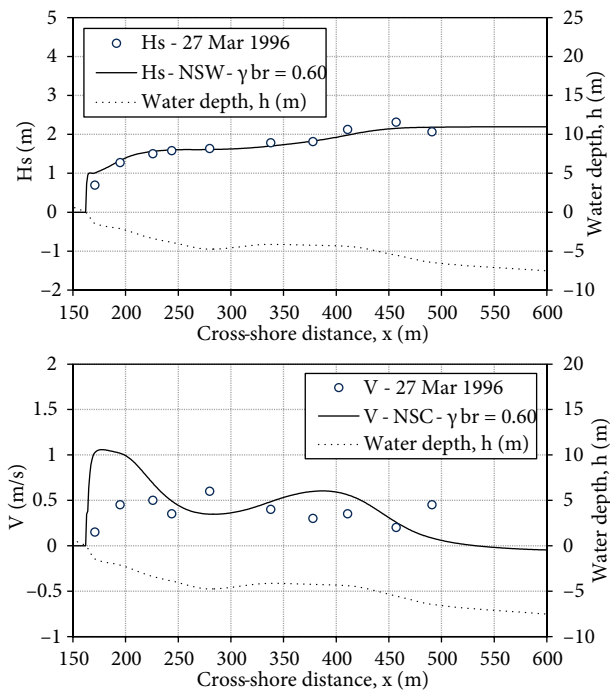


**Figure 4.** The measured and computed significant wave heights ( $H_s$ ) and longshore current velocities ( $V$ ) for the SANDYDUCK 27 March 1996 experiment.

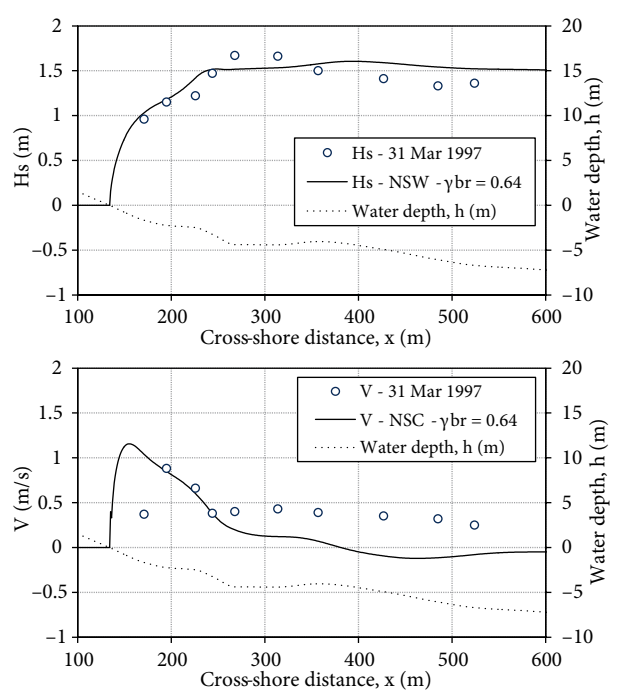


**Figure 6.** The measured and computed significant wave heights ( $H_s$ ) and longshore current velocities ( $V$ ) for the SANDYDUCK 31 March 1997 experiment.

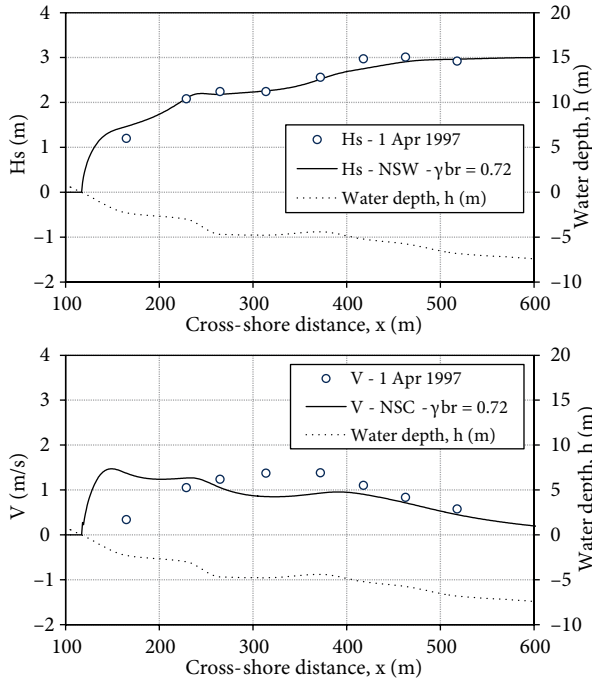


**Figure 7.** The measured and computed significant wave heights ( $H_s$ ) and longshore current velocities ( $V$ ) for the SANDYDUCK 1 April 1997 experiment.

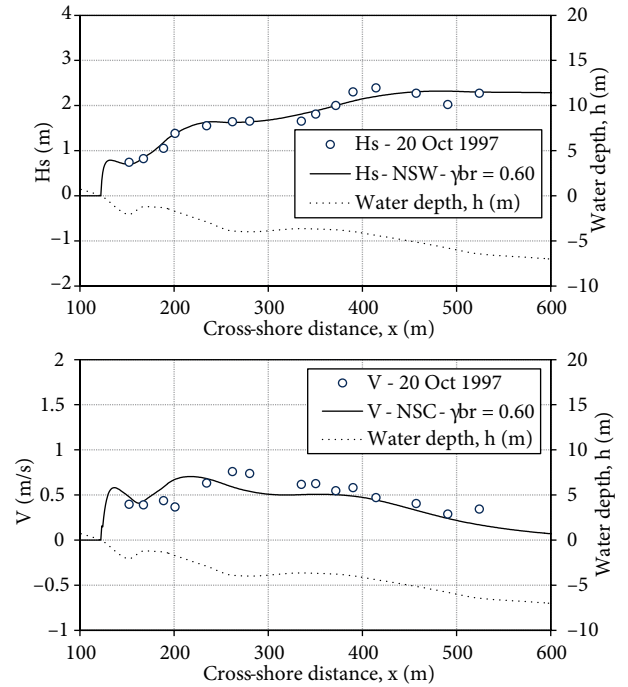


**Figure 9.** The measured and computed significant wave heights ( $H_s$ ) and longshore current velocities ( $V$ ) for the SANDYDUCK 20 October 1997 experiment.

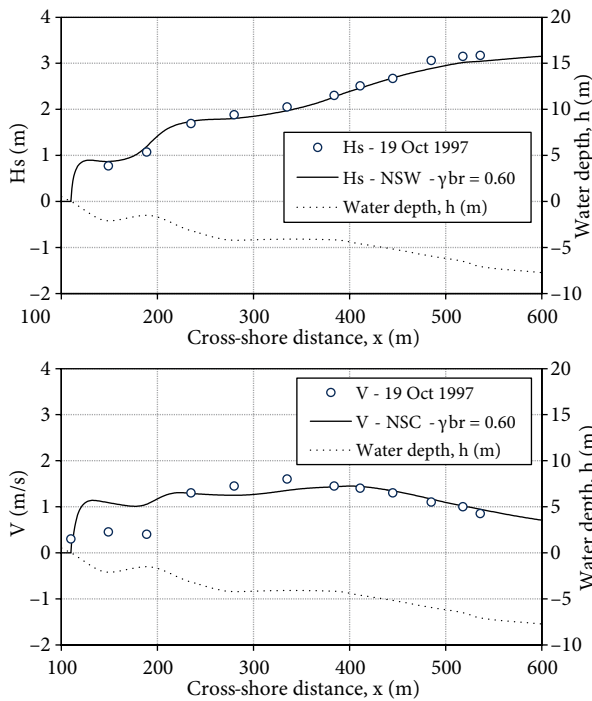


**Figure 8.** The measured and computed significant wave heights ( $H_s$ ) and longshore current velocities ( $V$ ) for the SANDYDUCK 19 October 1997 experiment.

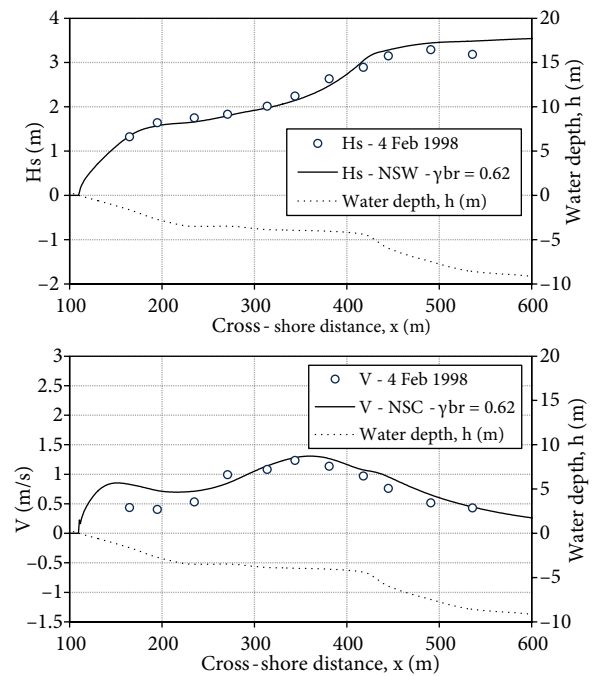


**Figure 10.** The measured and computed significant wave heights ( $H_s$ ) and longshore current velocities ( $V$ ) for the SANDYDUCK 4 February 1998 experiment.

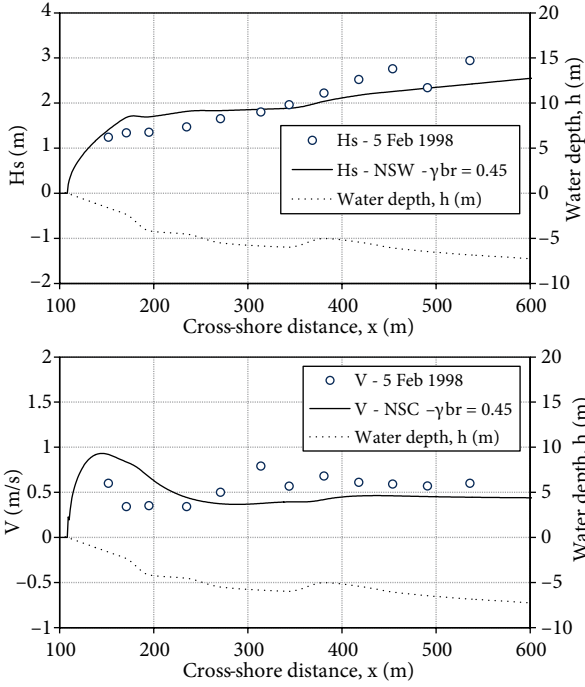


**Figure 11.** The measured and computed significant wave heights ( $H_s$ ) and longshore current velocities ( $V$ ) for the SANDYDUCK 5 February 1998 experiment.

to the beach cusps in nature. The water depths,  $h(x,y)$ , over the sinusoidal bathymetry in the benchmark problem are defined as:

$$h(x, y) = \begin{cases} 0.8 - x/20 & \text{for } x < 11 \text{ m and } x > 16 \text{ m} \\ 0.05 \left\{ (15 - x) - 0.75 \sin \left[ \frac{\pi(15 - x)}{5} \right] \right\} \left[ 1 + \sin \left( \frac{3\pi}{2} - \frac{2\pi y}{4} \right) \right] & \text{for } 11 \text{ m} \leq x \leq 16 \text{ m} \end{cases} \quad (27)$$

where  $x$  is the cross-shore coordinate (from 0 to 17 m) and  $y$  is the longshore coordinate (from 0 to 28 m) of the point of interest. The length between the sinusoidal beach cusps is taken as 4 m for the problem. The bottom slope beyond the 0.25-m water depth is taken as 1:20 up to the offshore boundary, where the water depth is 0.80 m. At the offshore boundary, unidirectional random waves with a significant wave height of 0.062 m and significant period of 1.0 s are generated perpendicular to the bottom contours. The breaker index is taken as  $\gamma_{br} = 0.78$ , bottom friction coefficient is taken as  $c_f = 0.015$ , energy transfer coefficient is taken as  $\alpha = 0.5$ , and effects of lateral mixing are disregarded in the simulation. The results of the simulation are shown in Figures 17 and 18.

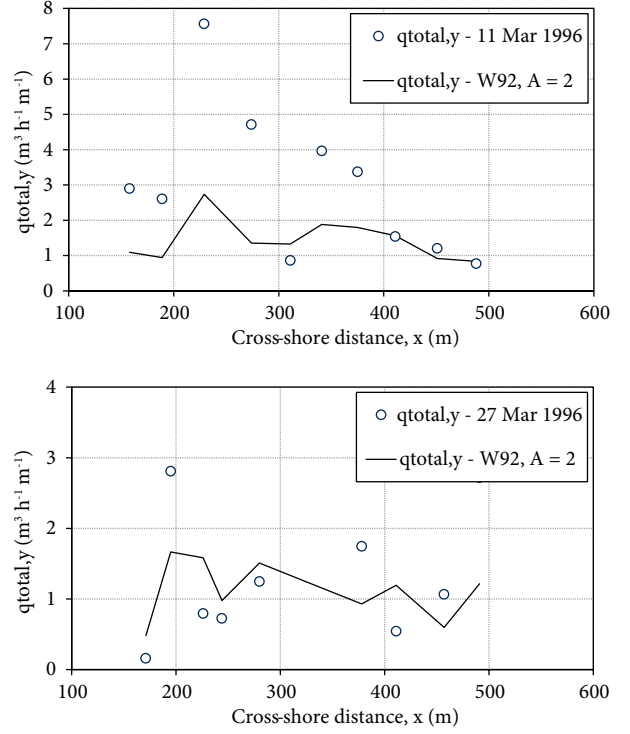


**Figure 12.** The measured and computed local total sediment transport rates ( $q_{total,y}$ ) for SANDYDUCK 11 March 1996 (top) and 27 March 1996 (bottom) experiments.

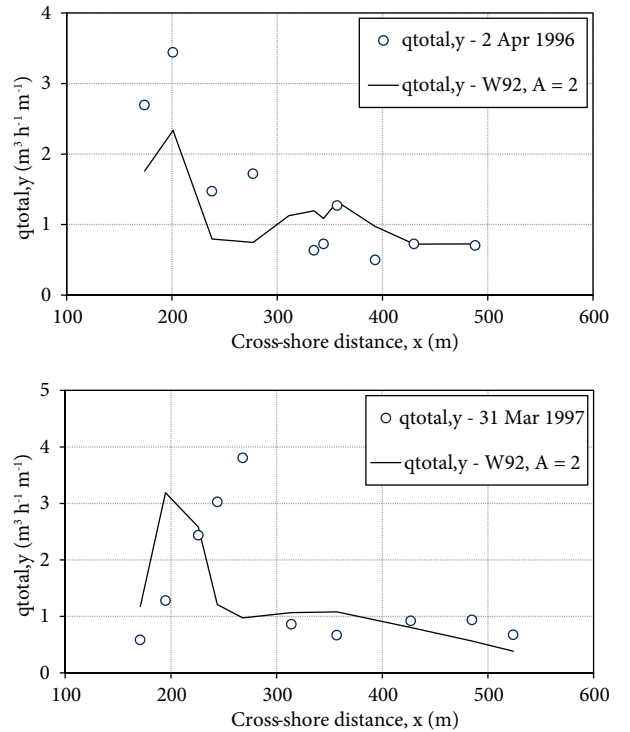


**Figure 13.** The measured and computed local total sediment transport rates ( $q_{total,y}$ ) for SANDYDUCK 2 April 1996 (top) and 31 March 1997 (bottom) experiments.

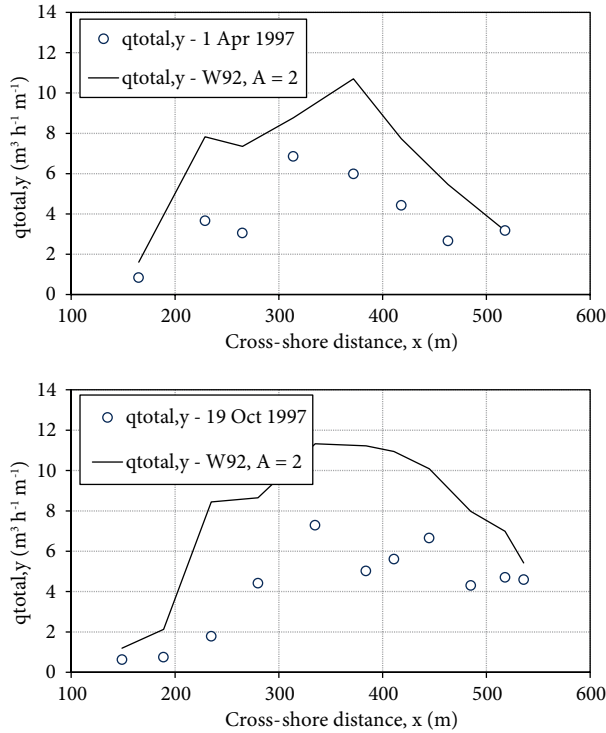


**Figure 14.** The measured and computed local total sediment transport rates ( $q_{total,y}$ ) for SANDYDUCK 1 April 1997 (top) and 19 October 1997 (bottom) experiments.

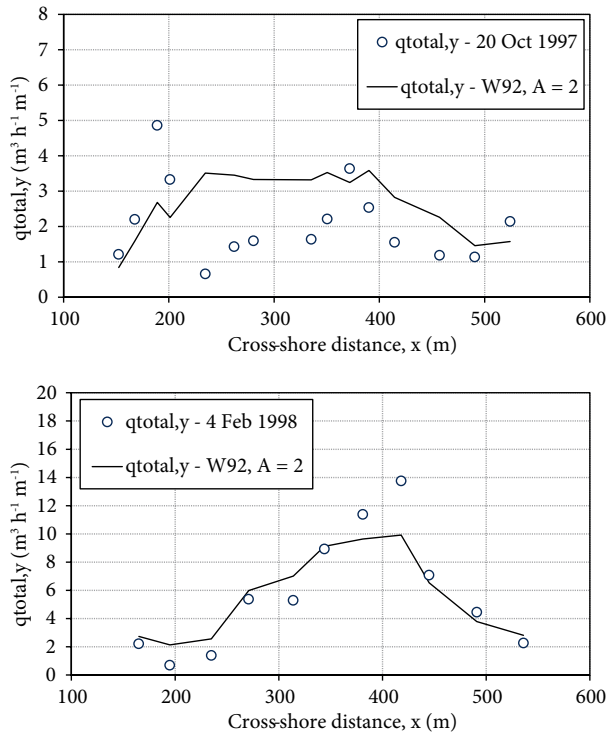


**Figure 15.** The measured and computed local total sediment transport rates ( $q_{total,y}$ ) for SANDYDUCK 20 October 1997 (top) and 4 February 1998 (bottom) experiments.

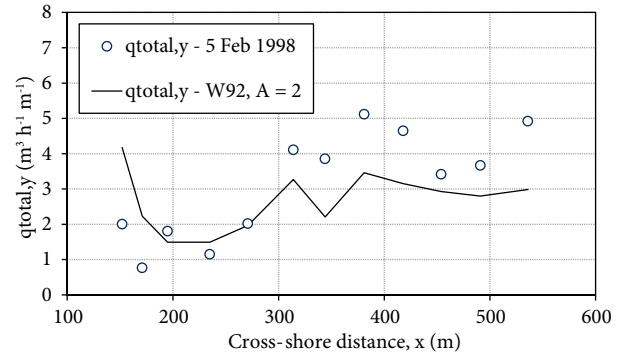


**Figure 16.** The measured and computed local total sediment transport rates ( $q_{total,y}$ ) for SANDYDUCK 5 February 1998 experiment.

As seen from Figure 17, the waves increase in height around cusps and the wave orthogonals converge to the cusps ( $x = 10, 14$ , and  $18$  m) as expected. The wave crests tend to align themselves with respect to bottom contours and decrease in height as the wave orthogonals diverge from each other. As seen from Figure 18, the rip currents are formed due to the diverted flows from the cusps such as in ranges of  $x = 11-13$  m and  $x = 15-17$  m.

### 3.2.2. Beach evolution around a single groin under oblique wave approach

To observe the behavior of the numerical beach evolution model (COD) in the case of a single groin under oblique wave approach on an initially straight shoreline with uniform bottom slope, a simulation with the COD model was performed. In the simulation, the deep water significant wave height is taken as  $H_{s0} = 2.0$  m, the significant wave period as  $T_s = 5.7$  s, the deep water mean approach angle as  $\theta = 30^\circ$ , and the grid spacing as 25 m in both  $x$ - and  $y$ -directions. The breaker index, eddy constant, bottom friction, surface roller constants, median grain size diameter, and  $A$  coefficient in the Watanabe (1992) formulation are taken as  $\gamma_{br} = 0.78$ ,  $\Lambda = 0.5$ ,  $c_f = 0.005$ ,  $\alpha =$

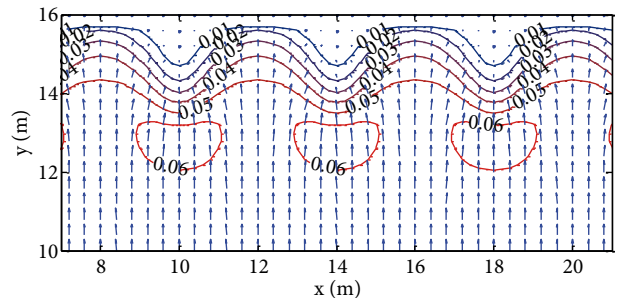


**Figure 17.** The vectorial representation of the computed wave field around beach cusps (arrows represent wave orthogonals and contour lines represent significant wave heights in meters).

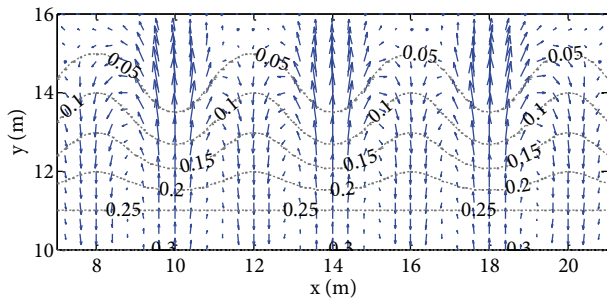


**Figure 18.** The vectorial representation of the computed current fields around the beach cusps (the arrows represent depth-averaged wave induced current velocities and the contour lines represent still water depths in meters).

0.5,  $d_{50} = 0.15$  mm, and  $A = 2$ , respectively. The length of the groin is taken as 500 m, reaching to a depth of 20 m on a 1:25 uniform bottom slope. The offshore water depth is taken as 50 m. The longshore extent of the computational domain is selected as 1625 m. The computed bottom contours after 200 h of simulation are given in Figure 19.

As seen from Figure 19, the shoreline recedes in the shadow zone of the structure and at the far upstream of the beach, and the bottom contours tend to align according to the shoreline. At the upstream of the groin, the accretion occurs and the shoreline moves offshore, confirming the expected bottom evolution around a single groin.

### 3.2.3. Beach evolution around a series of offshore breakwaters under oblique wave approach

To observe the behavior of the numerical beach evolution model (COD) in the case of a series of offshore breakwaters under oblique wave approach on an initially straight shoreline with uniform bottom slope (1:25), a simulation with the COD model was performed. In the simulation, the deep water significant wave height is taken as  $H_{s0} = 2.0$  m, the significant wave period as  $T_s = 5.7$  s, the deep water

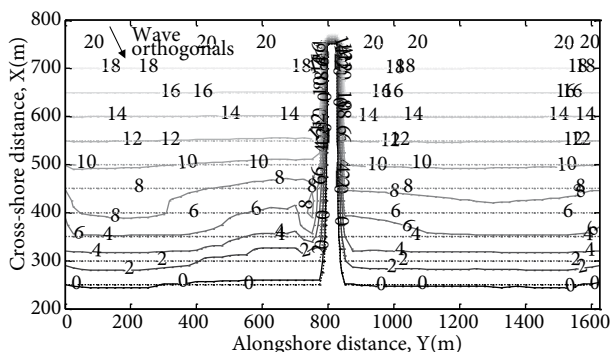


**Figure 19.** The change in the nearshore bathymetry around a single groin after 200 h of simulation (dashed lines represent the initial bottom contours, continuous lines represent the final bottom contours).

mean approach angle as  $\theta = 30^\circ$ , and the grid spacing as 25 m in both x- and y-directions. The breaker index, eddy constant, bottom friction, surface roller constants, median grain size diameter, and A coefficient in the Watanabe (1992) formulation are taken as  $\gamma_{br} = 0.78$ ,  $\Lambda = 0.5$ ,  $c_f = 0.005$ ,  $\alpha = 0.5$ ,  $d_{50} = 0.15$  mm, and  $A = 2$ , respectively. Three offshore breakwaters with a 150-m length and 150 m of spacing between them are located at a depth of 5 m, which is 125 away from the shoreline. The offshore water depth is taken as 50 m. The longshore extent of the computational domain is selected as 1625 m. The computed bottom contours after 200 h of simulation is given in Figure 20.

As seen from Figure 20, the accretion starts at the upstream end of the beach and the shoreline recedes at the downstream, the bottom contours are eroded between the breakwaters due to return flows, and the bottom contours move offshore behind the breakwaters due to current field behind the structures, confirming the expected bottom evolution around a series of offshore breakwaters.

## 4. Discussion

In this study, a 2D numerical model (COD) is constructed for the simulation of medium- to long-term (days, years) and meso- to macroscale (hundreds of meters to kilometers) morphological changes under the action of wind waves only over the arbitrary land and sea topographies around existing coastal structures and formations. The numerical model constructed is mainly composed of 4 main submodels. The first submodel is a phase-averaged spectral wave transformation model based on energy balance equation. The second submodel is a 2D depth-averaged numerical circulation model based on NSWs. The effects of surface rollers both in cross-shore and longshore directions are included in the nearshore circulation computations. The third submodel is a sediment transport model based on Watanabe's (1992)

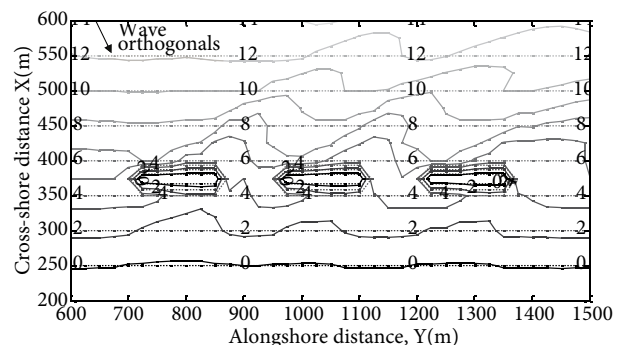


**Figure 20.** The change in the nearshore bathymetry around 3 offshore breakwaters after 200 h of simulation (dashed lines as initial bottom contours, continuous line as final bottom contours).



distributed total sediment load formulation. The fourth submodel is a bottom evolution model that computes the changes in the bottom topography based on the gradients of sediment transport rates over the computational domain and bottom avalanching. The numerical model differs from other 2DH beach evolution models in that it utilizes a directional spectrum without a frequency domain to decrease the computational load and a recent random wave breaking method proposed by Janssen and Battjes (2007) due to its easy implementation. The developed submodels are compared and validated with the datasets of field experiments by Miller (1999) and applied to some conceptual benchmark cases, including simulation of rip currents around beach cusps, beach evolution around a single shore perpendicular groin, and a series of offshore breakwaters. The model reflected the physical concepts well for the selected cases and was found to be capable of simulating some specific coastal processes like rip currents or formation of salients in the case of series of offshore breakwaters.

For further development of the numerical model, the enhancement of the numerical schemes utilized in the NSW and NSC models, the solution of an action balance equation instead of an energy balance to consider

wave-current interactions, implementation of more sophisticated methods for the computation of sediment transport rates including sediment transport in the swash zone, and inclusion of hard substrates in bed evolution are some of the major steps that need to be performed in order to enhance the applicability of the numerical model to irregular bathymetries and various cases of combinations of coastal structures and to acquire more numerically stable and quantitatively comparable solutions.

### Acknowledgments

The author would like to express his gratitude to Emeritus Prof Dr Yoshimi Goda, Prof Dr Leo van Rijn, and Atilla Bayram for their assistance in compiling and interpreting the datasets of the SANDYDUCK field experiments referred to in this study. The author would like to thank the editors and reviewers for their valuable time and comments, which overall improved the manuscript significantly. Finally, the author acknowledges that this study was partially supported by the Scientific and Technological Research Council of Turkey (TÜBİTAK), Research Grant No: 108M589, "Coastal Vulnerability Assessment to Climate Change Supported with A Numerical Sedimentation Model".

### LIST OF SYMBOLS

$A$	Empirical dimensionless parameter (Watanabe, 1992)	$H_{rms,0}$	Deep water root-mean-square wave height
$A_{sr}$	Surface roller area	$H_s$	Significant wave height
$A_x$	Lateral mixing term in $x$ -direction	$H_{s,0}$	Deep water significant wave height
$A_y$	Lateral mixing term in $y$ -direction	$H_{s,b}$	Significant breaking wave height
$B$	Tunable parameter to control the intensity of the dissipation due to wave breaking	$i$	Spatial grid index in $x$ -direction
$c_f$	Friction coefficient	$j$	Spatial grid index in $y$ -direction
$C$	Wave celerity	$k$	Wave number, also used as an assigned range to compute occurrence probability
$C_{g0}$	Deep water wave group celerity	$K_{sr}$	Energy dissipation rate of the surface roller
$C_0$	Deep water wave celerity	$L$	Wave length
$D_b$	Dissipation rate due to wave breaking	$L_0$	Deep water wave length
$D_d$	Dissipation term introduced by Mase (2001)	$m$	Bottom slope
$d$	Water depth from mean water level	$m_0$	Total wave energy density
$d_{50}$	Median grain size diameter	$n$	Ratio of group velocity to wave celerity, also used as time step index
$E$	Total wave energy	$q_{total,x}$	Total sediment transport rate in bulk volume including pores per unit longshore distance in cross-shore direction
$E_{sr}$	Kinetic energy of the surface roller	$q_{total,y}$	Total sediment transport rate in bulk volume including pores per unit cross-shore distance in longshore direction
$f$	Wave frequency	$s$	Degree of directional energy concentration
$f_c$	Current friction factor	$s_{max}$	Spreading parameter
$f_p$	Peak frequency	$s_{os}$	Deep water significant wave steepness
$f_w$	Wave friction factor	$S$	Directional wave spectral density
$F_x$	Sum of radiation stresses and stresses acting on the water body due to surface rollers in $x$ -direction	$S_{xx}$	Radiation stress acting in the $x$ -direction along $x$ -axis
$F_y$	Sum of radiation stresses and stresses acting on the water body due to surface rollers in $y$ -direction	$S_{xy}$	Radiation stress acting in the $y$ -direction along $x$ -axis
$g$	Gravitational acceleration	$S_{yx}$	Radiation stress acting in the $x$ -direction along $y$ -axis
$h$	Water depth from still water level	$S_{yy}$	Radiation stress acting in the $y$ -direction along $y$ -axis
$H$	Wave height		
$H_b$	Depth-limited maximum wave height		
$H_{rms}$	Root-mean-square wave height		



$T$	Wave period	$y$	Alongshore direction
$T_s$	Significant wave period	$\alpha$	Energy transfer coefficient
$T_p$	Peak wave period	$\gamma_b$	Breaker index
$u$	Depth-averaged current velocity in $x$ -direction	$\Delta t$	Time step in the nearshore circulation model
$u_0$	Maximum horizontal orbital velocity	$\Delta x$	Alongshore grid spacing
$v$	Depth-averaged current velocity in $y$ -direction	$\Delta y$	Offshore grid spacing
$v_x$	Energy flux propagation velocity in $x$ -direction	$\Delta t_m$	Time step in the bottom evolution model
$v_y$	Energy flux propagation velocity in $y$ -direction	$\varepsilon$	Fraction of the rate of dissipation in wave energy flux due to wave breaking
$v_\theta$	Energy flux propagation velocity in $\theta$ -direction	$\bar{\eta}$	Change in the mean water elevation
$x$	Cross-shore direction		

## References

- Ahrens JP (2000). The fall-velocity equation. *J Waterway Div-ASCE* 126: 99–102.
- Baldock TE, Holmes P, Bunker S, Van Weert P (1998). Cross-shore hydrodynamics within an unsaturated surf zone. *Coast Eng* 34: 173–196.
- Battjes JA (1975). Modeling of turbulence in the surf zone. *Modeling Techniques Symposium Proceedings* 2: 1050–1061.
- Baykal C (2012). Two-dimensional depth-averaged beach evolution modelling. PhD, Middle East Technical University, Ankara, Turkey.
- Baykal C, Ergin A, Güler I (2012). An energetic type model for the cross-shore distribution of total longshore sediment transport rate. In: *Proceedings of the ASCE 33rd International Conference on Coastal Engineering*. doi:10.9753/icce.v33.sediment.40.
- Bayram A, Larson M, Miller HC, Kraus NC (2001). Cross-shore distribution of longshore sediment transport: comparison between predictive formulas and field measurements. *Coast Eng* 44: 79–99.
- Bijker EW (1971). Longshore transport computations. *J Waterway Div-ASCE* 97: 687–703.
- Birkemeier WA, Donoghue C, Long CE, Hathaway KK, Baron CF (1997). The DELILAH Nearshore Experiment: Summary Data Report. Vicksburg, MS, USA: US Army Corps of Engineers, Waterways Experiment Station.
- Briand MHG, Kamphuis JW (1993). Sediment transport in the surf zone: a quasi 3-D numerical model. *Coast Eng* 20: 135–156.
- Bruneau N, Bonneton P, Pedreros R, Dumas F, Idier D (2007). A new morphodynamic modelling platform: application to characteristic sandy systems of the Aquitanian coast, France. *J Coast Res*, Special Issue 50: 932–936.
- Burkardt J (2010). Numerical Solution of the Shallow Water Equations, MATH 6425 Lectures 23/24. Blacksburg, VA, USA: ICAM/Information Technology Department, Virginia Polytechnic Institute and State University.
- Buttolph AM, Reed CW, Kraus NC, Ono N, Larson M, Camenen B, Hanson H, Wamsley T, Zundel AK (2006). Two-Dimensional Depth-Averaged Circulation Model CMS-M2D: Version 3.0, Report 2, Sediment Transport and Morphology Change. Technical Report ERDC/CHL TR-06-9. Vicksburg, MS, USA: Coastal and Hydraulics Laboratory, US Army Engineer Research and Development Center.
- Dabees MA, Kamphuis JW (1998). ONELINE, a numerical model for shoreline change. *Proceedings of the ASCE 27th International Conference on Coastal Engineering*, pp. 2668–2681.
- Dally WR, Dean RG, Dalrymple RA (1984). A model for breaker decay on beaches. *Proceedings of the ASCE 19th International Conference on Coastal Engineering*, ASCE, pp. 82–97.
- Dally WR, Brown CA (1995). A modeling investigation of the breaking wave roller with application to cross-shore current. *J Geophys Res* 100: 873–883.
- Dally WR, Dean RG, Dalrymple RA (1985). Wave height variation across beaches of arbitrary profile. *J Geophys Res* 90: 917–927.
- Danish Hydraulic Institute (2001). LITPACK Coastline Evolution, User's Guide and Reference Manual. Lyngby, Denmark: DHI.
- Ding Y, Wang SSY, Jia Y (2006). Development and validation of a quasi-three dimensional coastal area morphological model. *J Waterway Div-ASCE* 132: 462–476.
- Fredsoe J, Deigaard R (1994). *Mechanics of Coastal Sediment Transport*. Singapore: World Scientific.
- Goda Y (2006). Examination of the influence of several factors on longshore current computation with random waves. *Coast Eng* 53: 157–170.
- Goda Y (2010). *Random Seas and Design of Maritime Structures*. 3rd ed. Singapore: World Scientific.
- Hanson H, Kraus NC (1989). GENESIS: Generalized Model for Simulating Shoreline Change. Tech. Rep. CERC-89-19, Report 2 of a Series, Workbook and User's Manual. Vicksburg, MS, USA: US Army Corps of Engineers, Waterways Experiment Station.
- Janssen TT, Battjes JA (2007). A note on wave energy dissipation over steep beaches. *Coast Eng* 54: 711–716.
- Kuroiwa M, Matsubara Y, Kuchiishi T, Kato K (2006). Prediction system of 3D beach evolution with 2DH and Q-3D hydrodynamic modes. *Proceedings of the 16th International Offshore and Polar Engineering Conference*, pp. 751–757.
- Larson M, Kraus NC (1991). Numerical model of longshore current for bar and trough beaches. *J Waterway Div-ASCE* 117: 326–347.
- Larson M, Kraus NC (2002). NMLONG: Numerical Model for Simulating Longshore Current; Report 2: Wave-Current Interaction, Roller Modeling, and Validation of Model Enhancements. Technical Report ERDC/CHL TR-02-22. Vicksburg, MS, USA: US Army Engineer Research and Development Center.

- Lax PD, Wendroff B (1960). Systems of conservation laws. *Comm Pure Appl Math* 13: 217–237.
- Longuet-Higgins MS (1970). Longshore current generated by obliquely incident sea waves, 1 & 2. *J Geophys Res* 75: 6779–6801.
- Mase H (2001). Multidirectional random wave transformation model based on energy balance equation. *Coast Eng* 43: 317–337.
- Militello A, Reed CW, Zundel AK, Kraus NC (2004). Two-Dimensional Depth-Averaged Circulation Model M2D: Ver. 2.0, Report 1: Documentation and User's Guide, ERDC/CHL TR-04-02. Vicksburg, MS, USA: US Army Engineer Research and Development Center.
- Miller HC (1999). Field measurements of longshore sediment transport during storms. *Coast Eng* 36: 301–321.
- Mitsuyasu H, Suhaya T, Mizuno S, Ohkuso M, Honda T, Rikiishi K (1975). Observations of the directional spectrum of ocean waves using a cloverleaf buoy. *J Phys Oceanogr* 5: 750–760.
- Nam PT, Larson M, Hanson H (2010). Modeling morphological evolution in the vicinity of coastal structures. *Proceedings of the ASCE 32nd International Conference on Coastal Engineering*. doi:10.9753/icce.v32.sediment.68.
- Nam PT, Larson M, Hanson H, Hoan LX (2009). A numerical model of nearshore waves, currents, and sediment transport. *Coast Eng* 56: 1084–1096.
- Nielsen P (1992). *Coastal Bottom Boundary Layers and Sediment Transport*. Singapore: World Scientific.
- Park KY, Borthwick AGL (2001). Quadtree grid numerical model of nearshore wave-current interaction. *Coast Eng* 42: 219–239.
- Pelnard-Considere R (1956). Essai de theorie de l'evolution des formes de rivage en Plage de Sable et de Galets. 4th J l'Hydraulique, Les Energies de la Mer, Question III, Rapport No. 1: 289–298 (in French).
- Perenne N (2005). MARS: A Model for Applications at Regional Scale, Documentation Scientifique Ver. 1.0, User Manual. Issy-les-Moulineaux, France: Institut français de recherche pour l'exploitation de la mer
- Reeve D, Chadwick A, Fleming C (2004). *Coastal Engineering: Processes, Theory and Design Practice*. Abingdon, UK: Spon Press, Taylor & Francis Group.
- Roelvink D, Reniers A, van Dongeren A, van Thiel de Vries J, McCall R, Lescinski J (2009). Modelling storm impacts on beaches, dunes and barrier islands. *Coast Eng* 56: 1133–1152.
- Saint-Cast F (2002). Modélisation de la morphodynamique des corps sableux en milieu littoral. PhD, University of Bordeaux, Bordeaux, France (in French).
- Shimizu T, Kumagai, T, Watanabe A (1996). Improved 3-D beach evolution model coupled with the shoreline model (3D-shore). *Proceedings of the ASCE 25th International Conference on Coastal Engineering*, pp. 2843–2856.
- Syme WJ (1991). Dynamically linked two-dimensional/one-dimensional hydrodynamic modeling program for rivers, estuaries & coastal waters. MSc, University of Queensland, Queensland, Australia.
- Tajima Y, Madsen OS (2003). Modeling near-shore waves and surface rollers. *Proceedings of the 2nd International Conference on Asian and Pacific Coasts*. Paper No. 28.
- Takayama T, Ikeda N, Hiraishi T (1991). Wave transformation calculation considering wave breaking and reflection. *Report of the Port and Harbor Res Inst* 30: 21–67 (in Japanese).
- Van Rijn LC (1990). *Handbook Sediment Transport by Currents and Waves*. Report H461. Delft, the Netherlands: Delft Hydraulics.
- Van Rijn LC (2004). Longshore sediment transport. Report Z3054.20. Delft, the Netherlands: Delft Hydraulics.
- Warner JC, Sherwood CR, Signell RP, Harris CK, Arangoc HG (2008). Development of a three-dimensional, regional, coupled wave, current, and sediment-transport model. *Comput Geosci* 34: 1284–1306.
- Watanabe A (1992). Total rate and distribution of longshore sand transport. *Proceedings of the ASCE 25th International Conference on Coastal Engineering*, pp. 2528–2541.